Geophysica (2025), 60 (1), 25–40

Application of SRP–PHAT beamforming in seismology

Alexander Varypaev[1,*]

[1]Institute of Mathematics and Informatics, Bulgarian Academy of Science
[*]Corresponding mail address, avalex89@gmail.com

(Submitted: 2024-07-10; Accepted: 2026-04-15)

Abstract

The Steered Response Power – Phase Transform (SRP–PHAT) method, originally developed in acoustics for robust source localization in noisy and reverberant environments, is evaluated for applications to small-aperture seismic arrays. This study demonstrates that SRP–PHAT can effectively address two related tasks: microseismic source localization and frequency–wavenumber (f–k) spectrum estimation. A theoretical framework is provided, highlighting the conceptual similarity between these tasks, followed by experimental validation using real seismic data. Three different datasets are analyzed: (1) recordings of the S phase from the Kursk submarine explosion (August 12, 2000) captured by the ARCES array; (2) data from a temporary array deployed for tremor source monitoring; (3) data from a seismic array used in microseismic monitoring during hydraulic fracturing. The results illustrate several cases in which SRP–PHAT provides more stable or accurate slowness estimates than conventional methods, suggesting that it represents a viable alternative to classical f–k approaches, without claiming universal superiority.

Keywords: array signal processing; slowness estimation; seismic source localization; phase transform; small-aperture array; semblance; SRP–PHAT

1 Introduction

The primary purpose of antenna arrays is to collect data by sampling a wavefield generated by a finite number of signal sources. These time series can then be used for further interpretation of the observed physical processes and for estimating important parameters. In recent years, antenna arrays have found applications in acoustics, seismology, radio astronomy, radar, and sonar systems (e.g., *Monzingo et al.*, 2011; *Dai and Sun*, 2023; *Brokešová and Málek*, 2018). Since the propagation of waves and their registration on array sensors can often be described by the same mathematical observation model, and because signal distortion due to additive noise is a common problem, it is valuable to explore new and efficient developments in array signal processing across related fields.

For accurate sound source localization, the phase-based algorithm SRP–PHAT (The Steered Response Power – Phase Transform) was developed and has proven to be highly robust to ambient noise and reverberation, which are the main causes of distortion in the target source signal (*Silverman et al.*, 2005; *Brandstein and Ward*, 2001). The method has been extensively studied in acoustics and signal processing, with numerous works devoted to its theoretical development and applications (*Grinstein et al.*, 2024). Experience with phase-based algorithms in various areas of information technology, such as communications and acoustics, shows that these algorithms are robust not only to external interference but also to deviations of assumed wave propagation parameters from their actual values. Such deviations often appear when processing signals embedded in noise. Phase algorithms suppress this noise through averaging more effectively than methods operating directly on the raw observations. Moreover, SRP–PHAT is a beamforming technique, requiring that observed signals from a point source remain coherent across array sensors.

Array signal processing presents similar challenges in seismology, where signals recorded at small-aperture arrays (typically 0.5 km to 3 km) are often corrupted by natural or anthropogenic noise, or by the coda of other seismic phases. In these arrays, the short distances between sensors generally preserve signal coherence, making SRP–PHAT suitable for estimating important parameters, depending on the problem at hand, including near-field or far-field source localization. Here, the term ‘seismic array’ refers by default to a small-aperture array.

Near-field source localization is relevant for monitoring microseismic events that generate complex wavefields in the elastic Earth at distances comparable to the array aperture. Typical examples include: (1) monitoring hydraulic fracturing in terrestrial environments, a critical and costly operation in oil and gas field development (*Duncan and Eisner*, 2010), (2) monitoring mining-induced seismicity and rock fracturing, which is important for mine safety management (*Liu et al.*, 2024), (3) seismic monitoring of hydrothermal activity to optimize geothermal energy extraction (*Azzola and Gaucher*, 2024; *Legaz et al.*, 2009). Conventional and relatively recent methods for microseismic monitoring in these applications include Semblance analysis (*Duncan et al.*, 2010; *Staněk et al.*, 2015). In the experimental part of this study, the location capabilities of Semblance and SRP–PHAT are compared for microseismic sources with explosion-type focal mechanisms and low signal-to-noise ratios.

Far-field seismic sources are those located sufficiently far from the array so that their wavefronts can be approximated as planar when recorded by array sensors. Estimating the coordinates of such events is important in applications such as: (1) monitoring and tracking volcanic tremor sources (*Eibl et al.*, 2017), (2) surveillance of underground nuclear tests (*Husebye and Dainty*, 1995), (3) determining coordinates of regional events, such as earthquakes or industrial explosions (*Eisermann et al.*, 2018). Experience with modern automatic seismic monitoring systems shows that location uncertainty can be significantly reduced by incorporating information on the arrival directions of seismic waves at array sensors, i.e., by accurately estimating the slowness vector and backazimuth. Traditionally, this has been achieved using classic frequency–wavenumber (CFK) analyses applied to array recordings (*Kennett*, 2002; *Kværna and Ringdal*, 1986), rather than through polarization analysis of single three-component sensors. Nevertheless, monitoring low-magnitude seismicity remains an open challenge, motivating the application of new array signal processing techniques. For this purpose, SRP–PHAT was applied to real seismic array records to estimate the plane-wave slowness vector, and the results were compared with those obtained from conventional methods.

2 *Mathematical model of observations*

In both near-field and far-field source scenarios, the signals generated by seismic source and recorded by seismic array sensors can be represented as outputs of a multi-dimensional linear system with one input and several outputs (for the finite and discrete time) (*Aki and Richards*, 2009; *Varypaev*, 2024):

$$\mathbf{u}_k = \mathbf{h}_k * s_k + \boldsymbol{\xi}_k \ , \quad k \in \overline{1,n} \ , \tag{2.1}$$

where $\mathbf{h}_k * s_k$ is the convolution of the time series; the vector time series $\mathbf{u}_k = \mathbf{u}(k/f_d)$ are discrete observations of seismic array, f_d the sampling frequency; s_k is the waveform of the seismic wave affecting the array; $\mathbf{h}_k(\boldsymbol{\theta}) * s_k$ are the outputs of the linear system, i.e. registered source signals; $\mathbf{h}_k(\boldsymbol{\theta}) = \left(h_{k,1}(\boldsymbol{\theta}), \ldots, h_{k,m}(\boldsymbol{\theta})\right)^\top$ is the impulse response function describing wave propagation through a solid medium between seismic source and array sensors; $\boldsymbol{\xi}_k = \left(\xi_{k,1}, \ldots, \xi_{k,m}\right)^\top$ are Gaussian stationary processes with a zero vector of average values. It is also assumed that noise components are incoherent between any pair of sensors. $\boldsymbol{\theta} = (\theta_1, \ldots, \theta_p) \in \boldsymbol{\Theta} \subset \mathbb{R}^p$, $p \in \mathbb{N}$ is the unknown vector parameter of the linear system to be estimated in relation to considered problem.

For mathematical and practical reasons, it is convenient to transform discrete observations $\mathbf{u}_k$, $k \in \overline{1,n}$ into the frequency domain using discrete finite Fourier transform (DFFT): $\mathbf{u}_k \Leftrightarrow \dot{\mathbf{u}}_j$, where

$$\dot{\mathbf{u}}_j = \left(u_{j,1}, \ldots, u_{j,m}\right)^\top = \frac{1}{\sqrt{n}} \sum_{k=1}^{n} \mathbf{u}_k \exp\left\{-\frac{2i\pi jk}{n}\right\}, \quad j \in \overline{1,n} \tag{2.2}$$

then according to similar DFFT transformations $\mathbf{h}_k(\boldsymbol{\theta}) \Leftrightarrow \dot{\mathbf{h}}_j(\boldsymbol{\theta})$, $s_k \Leftrightarrow \dot{s}_j$, $\boldsymbol{\xi}_k \Leftrightarrow \dot{\boldsymbol{\xi}}_j$ we can write out the model of array observation (1) in the frequency domain of DFFT

$$\dot{\mathbf{u}}_j = \dot{\mathbf{h}}_j(\boldsymbol{\theta})\dot{s}_j + \dot{\boldsymbol{\xi}}_j + \dot{\mathbf{o}}_j(1/\sqrt{n}) \ , \quad \max_{1 \le j \le N} |\dot{\mathbf{o}}_j(1/\sqrt{n})| \to 0 \ . \tag{2.3}$$

Incoherence of noise components in this case will mean that matrix power spectral density $\mathrm{E}\left[\dot{\boldsymbol{\xi}}_j \dot{\boldsymbol{\xi}}_j^*\right] = \dot{\mathbf{F}}_j$ is diagonal. Here sign '$*$' denotes conjugation and transpose operation.

3 *SRP–PHAT estimator of unknown parameter* $\boldsymbol{\theta}$

The most effective computational procedures for averaging noise in determining the parameters of observed signals are synthesized by methods of mathematical statistics: for given probabilistic parametric observation models, statistical estimation theory makes it possible to find estimates of signal parameters that are the best in terms of a certain quality criterion, for example, the standard deviation of the estimate from the true value of the parameter. In this sense, model (2.3) can be used to derive the phase-based SRP–PHAT estimator (*Varypaev and Kushnir*, 2020; *Zhang et al.*, 2008):

$$\dot{\boldsymbol{\theta}} = \arg\max_{\boldsymbol{\theta}\in\Theta} \sum_{j=1}^{n} \left| \sum_{k=1}^{m} \frac{\dot{u}_{j,k}}{|\dot{u}_{j,k}|} \dot{h}_{j,k}(\boldsymbol{\theta}) \right|^2 , \tag{3.1}$$

where frequency response function $\dot{\mathbf{h}}_j(\boldsymbol{\theta})$ has the form

$$\dot{\mathbf{h}}_j(\boldsymbol{\theta}) = \big(\exp(-2\pi i f_j \tau_k(\boldsymbol{\theta})), \quad k \in \overline{1,m}\big)^\top , \quad f_j \in [0, f_d/2] . \tag{3.2}$$

In the general sense, variable $\tau_k(\boldsymbol{\theta})$ is a certain function depending on the unknown parameter $\boldsymbol{\theta}$.

Consider the case of a plane wave arriving on the seismic array, then $\boldsymbol{\theta} = (\theta_1, \theta_2) \in \boldsymbol{\Theta} \subset \mathbb{R}^2$ is the slowness vector, and the following expressions hold:

$$\tan\alpha = \frac{\theta_2}{\theta_1} , \quad |\boldsymbol{\theta}| = \sqrt{\theta_1^2 + \theta_2^2} , \quad \sin\beta = \frac{1}{V_\mathrm{p}|\boldsymbol{\theta}|} , \tag{3.3}$$

where α is the azimuth, β is the angle of incidence, V_p is seismic P-wave velocity near the Earth's surface (it can also be V_s, seismic S-wave velocity, or something else depending on what seismic phase is processed). Vector $\boldsymbol{\theta}$ is the most convenient quantity to characterize the arrival direction of a plane wave. Value equal to $1/\boldsymbol{\theta}$ is the apparent velocity vector. It follows from the equalities (3.3) that the estimation of $\boldsymbol{\theta}$ furnishes important information for dealing with the key problem of seismic monitoring, namely, earthquake location. When denoting array sensor coordinates in a rectangular system as (x_k, y_k, z_k), $\tau_k(\boldsymbol{\theta})$ can be calculated as time delays of plane wave propagation from point $(0,0)$ to k^{th} array sensor:

$$\tau_k(\boldsymbol{\theta}) = \theta_1 x_k + \theta_2 y_k , \quad k \in \overline{1,m} \tag{3.4}$$

When a seismic source is located sufficiently close to a seismic array, the wavefront of observed wave is significantly different from a flat one. For simplicity, consider the case of a spherical wave, generated by seismic source in homogeneous media with a certain velocity propagation of P-waves V_p, then the unknown parameter of the model (2.3) is $\boldsymbol{\theta} = (\theta_1, \theta_2, \theta_3)$, i.e., the source coordinates. Functions $\tau_k(\boldsymbol{\theta})$ will have the following form in this case:

$$\tau_k(\boldsymbol{\theta}) = \sqrt{(x_k - \theta_1)^2 + (y_k - \theta_2)^2 + (z_k - \theta_3)^2}/V_\mathrm{p} , \quad k \in \overline{1,m} \tag{3.5}$$

In the most common case, when the medium of wave propagation between the source and seismic array is inhomogeneous, i.e., $V_\mathrm{p} = V_\mathrm{p}(x,y,z) \neq \text{const}$, functions $\tau_k(\boldsymbol{\theta})$ will have a more complex analytical form:

$$\tau_k(\boldsymbol{\theta}) = \int_{L_{\mathrm{k},\boldsymbol{\theta}}} \frac{\mathrm{d}l}{V_\mathrm{p}(x,y,z)} \tag{3.6}$$

Above, $L_{k,\boldsymbol{\theta}}$ is the transition distance of the seismic ray connecting the seismic source and the k^{th} sensor.

Using equations (3.1)–(3.4) allows to estimate the slowness vector while formulas (3.1), (3.2), (3.5)–(3.6) allow to determine the location of a seismic source. Thus, we can conclude that the estimator (3.1) can be applied to observations of array sensors to solve two different seismological problems. In the sense of point theory estimation and mathematical model of observations (2.3), they are identical, however.

4 *Frequency-wavenumber analyses (f–k) of regional event from ARCES array data*

In this study, seismic recordings of the explosion associated with the submarine accident on August 12, 2000 in the Barents Sea are analyzed. The origin time of the main explosion is approximately 07:30:41.7 UTC and the Richter magnitude is equal to 3.5. Data from the ARCES seismic array are used for the analysis. The array geometry and the relative geographical configuration of the source and receivers are shown in Fig. 4.1. Seismograms of the recorded Pn, Pg, and Sn phases are presented in Fig. 4.2.

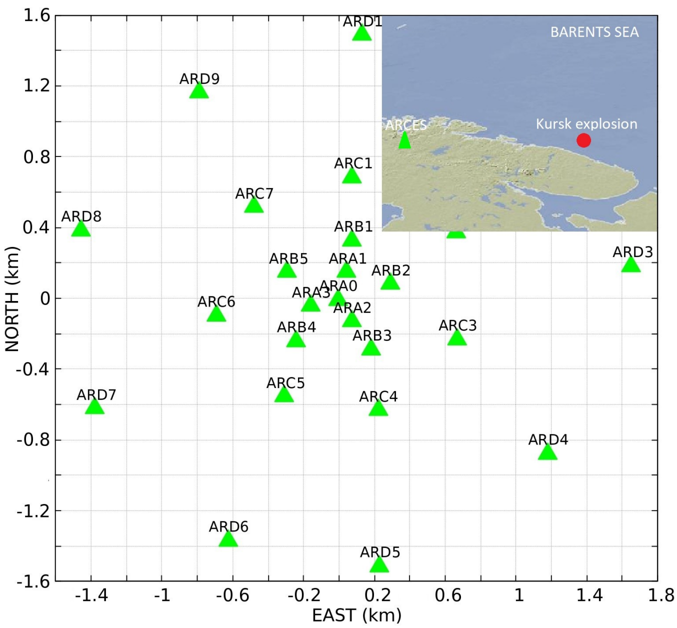

Fig. 4.1: ARCES array geometry. Explosion of Kursk submarine from 12 Aug 2000 denoted by red point.

It should be noted that the timing indicated on the seismograms is given in UTC and follows the NORSAR event location estimates. This timing is consistent with the waveform dataset used in the present study and may differ from origin times reported in other studies due to differences in data and processing approaches.

The comparison of slowness vector estimation methods is performed for the same time interval corresponding to the Sn phase using two approaches: the proposed SRP–PHAT algorithm and the classical frequency–wavenumber method (CFK). The Sn phase is of particular interest due to its complex propagation characteristics. It propagates within the uppermost mantle and is strongly influenced by lateral heterogeneities, attenuation, and scattering effects. As a result, Sn waveforms typically exhibit pronounced coda and

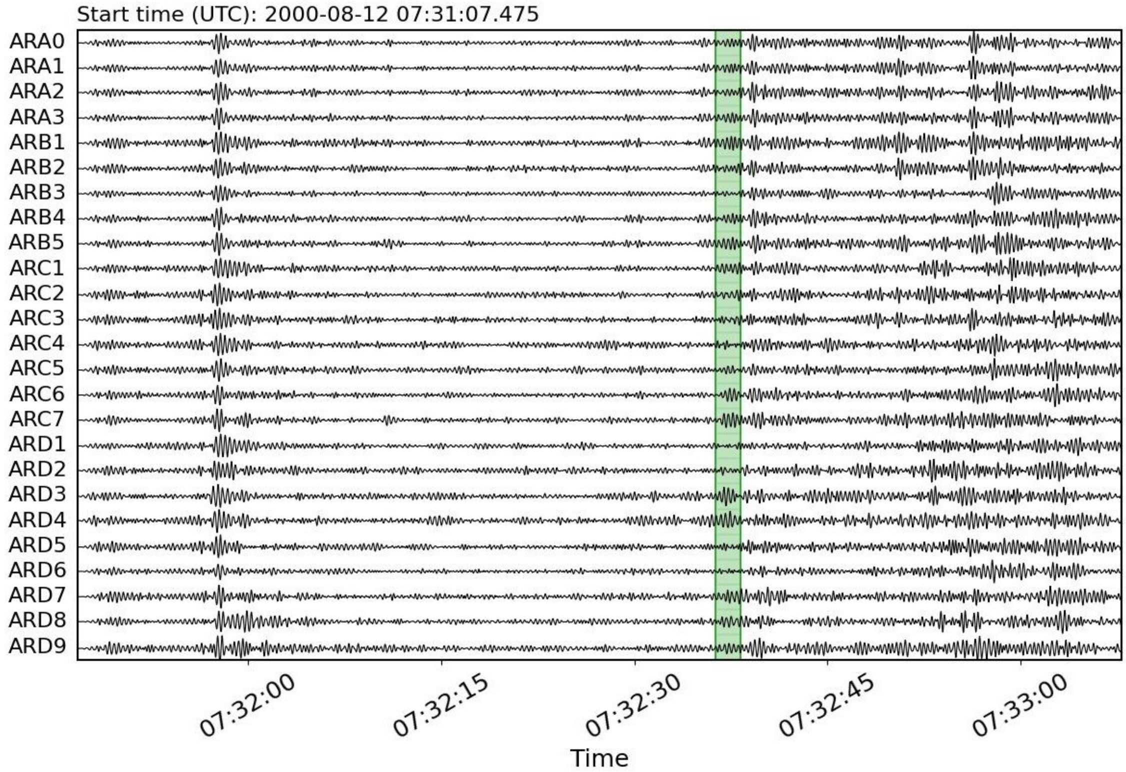

Fig. 4.2: Multichannel seismogram of earthquake waveform from 12 Aug 2000 with its Pn, Pg, and Sn waves recorded on the vertical 'shz' component of seismic array sensors. Green color highlights processed interval of Sn phase.

reduced spatial coherence across array sensors. This makes the Sn phase an excellent test case for evaluating the robustness of different slowness estimation techniques under conditions of degraded inter-sensor correlation.

f–k maps obtained using both methods for two different frequency bands (2 Hz to 10 Hz and 5 Hz to 10 Hz) are shown in Fig. 4.3. The first column corresponds to the SRP–PHAT method, while the second column presents the results of the CFK method. All processing parameters, including the time window and frequency bands, are identical for both methods and are explicitly indicated in the figures.

The SRP–PHAT method provides stable and consistent estimates of the backazimuth for both frequency bands, yielding values of approximately 86°. This estimate is in good agreement with the backazimuth obtained from P-wave analysis using the CFK method in the work *Gibbons and Ringdal* (2006), where the high spatial coherence of P-wave signals ensures reliable estimation. In addition, SRP–PHAT produces nearly identical estimates of apparent velocity, approximately $6\,\mathrm{km\,s^{-1}}$, for both frequency bands.

In contrast, the CFK method demonstrates significant variability and instability in the estimation results. For the 2 Hz to 10 Hz band, the estimated backazimuth is 78.1°, while for the 5 Hz to 10 Hz band it changes to 95.7°, indicating a strong dependence on the selected frequency range. Furthermore, for the 5 Hz to 10 Hz band, the apparent velocity estimated by CFK reaches $9.95\,\mathrm{km\,s^{-1}}$, which is physically inconsistent with expected Sn wave velocities and significantly exceeds realistic values for S-wave propagation.

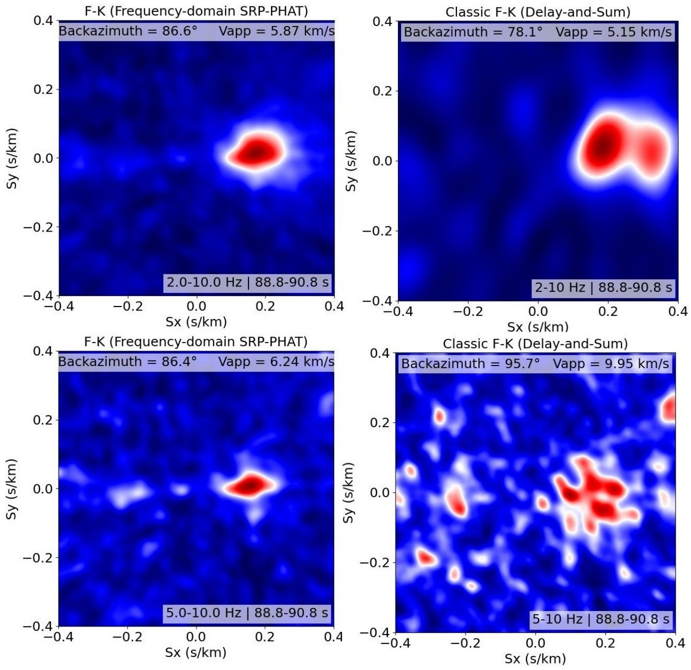

Fig. 4.3: f–k maps for the Sn phase obtained using SRP–PHAT (left column) and CFK (right column) methods for two frequency bands: 2 Hz to 10 Hz and 5 Hz to 10 Hz. Processing parameters, including the time window and frequency bands, are identical for both methods and are indicated in the figures. Time intervals in seconds is being counted from start time (UTC) of seismogram denoted at the top of Fig. 4.2, i.e., `2000-08-12T07:31:07.475`.

Thus, the discrepancies and instability in slowness estimation obtained using the CFK method are substantial. This behavior can be attributed to the reduced spatial coherence of the Sn phase, which negatively affects conventional beamforming techniques.

In addition to the numerical differences, the quality of the resulting f–k maps also differs significantly between the two methods. The CFK maps are characterized by low resolution in terms of the ratio between the dominant maximum and secondary extrema (*Schweitzer et al.*, 2012), indicating ambiguity in identifying the true slowness vector. In contrast, the SRP–PHAT maps exhibit a more pronounced global maximum, reflecting improved robustness to signal decorrelation.

Overall, this example provides a clear, albeit single, demonstration of the robustness of the SRP–PHAT method when applied to real seismic array data, particularly under challenging conditions associated with complex wave propagation and reduced inter-sensor coherence.

5 *Volcanic tremor analyses using 2 hours data of temporary 5L seismic array*

In this section, we use seismic array data previously analyzed by *Eibl et al.* (2017) and apply the SRP–PHAT method to the same dataset in order to compare the obtained results with those reported in the original study. Volcanic tremor is a persistent seismic signal generated by microseismicity associated with volcanic disturbances and is often associated with the movement of magmatic fluids in the subsurface. Determining the coordinates of its source in real time is important for reducing the volcanic risk. Seismic array data allows to estimate the backazimuth and slowness in overlapping time windows, which helps to track the location of volcanic tremor sources. Traditional travel time location methods cannot be used to locate tremor sources, since tremor has no clear P- and S-wave arrivals. In contrast, two or more arrays allow a determination of the epicentral location of the source.

A temporary seismic array with network code 5L, originally deployed and described in *Eibl et al.* (2017), was used for monitoring and tracking tremor sources during subglacial floods and volcanic eruptions at the Vatnajökull ice cap in Iceland. The array geometry and the approximate propagation path of the volcanic dyke below the glacier is shown in Fig. 5.1, as well as array geometry.

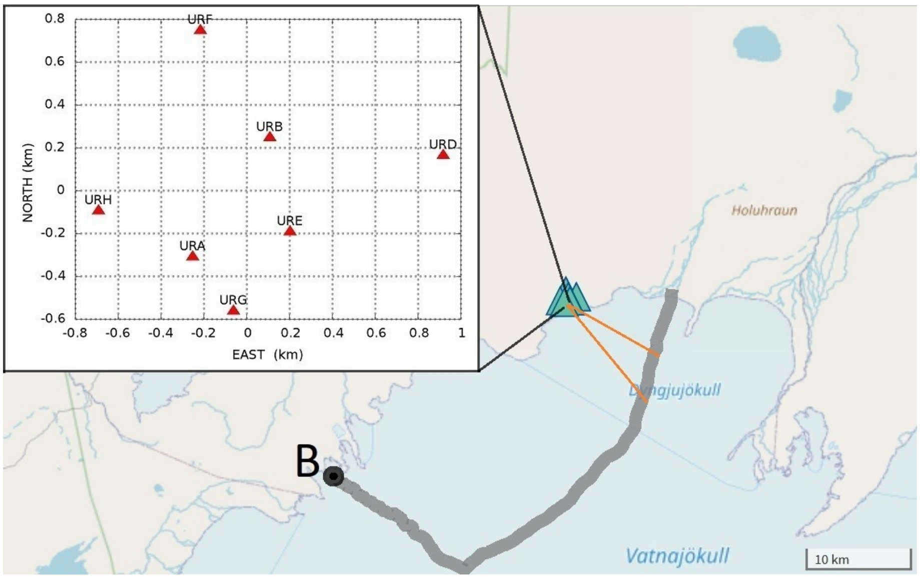

Fig. 5.1: Location and geometry of the seven station 5L seismic array deployed to collect data during the 2014–2015 eruption at Bárðarbunga volcano in Iceland. The location of Bárðarbunga volcano is indicated by the black letter B. Grey line is a volcanic dyke. Orange lines indicate the estimated (by SRP–PHAT) area of backazimuth of microseismic events caused by volcanic tremor for 2 h.

The volcanic tremor started on 3 September of 2014 around midnight and ended abruptly at 21:35 and was studied in *Eibl et al.* (2017). Two hours of the seismic array data were used to carry out an f–k analysis of the microseismicity caused by volcanic tremor Fig. 5.2.

We follow the processing strategy described in *Eibl et al.* (2017), while applying the SRP–PHAT method to the same dataset, except for some parameters like frequency band and time window length. Spectral-temporal analysis of seismograms (Fig. 2d in *Eibl et al.*, 2017) shows the presence of signal mostly in the range from 0.9 Hz to 2.0 Hz. Note that while signal energy is also present below 0.9 Hz, this lower-frequency content was not considered, as it does not significantly contribute to the estimation of slowness and backazimuth in our analysis. That is why all data of seismic array was downsampled to 20 Hz. All 2 h of multichannel seismogram is subdivided into 70% overlapping time windows that were 10 periods long – 7.8 s that corresponding to frequency with the highest

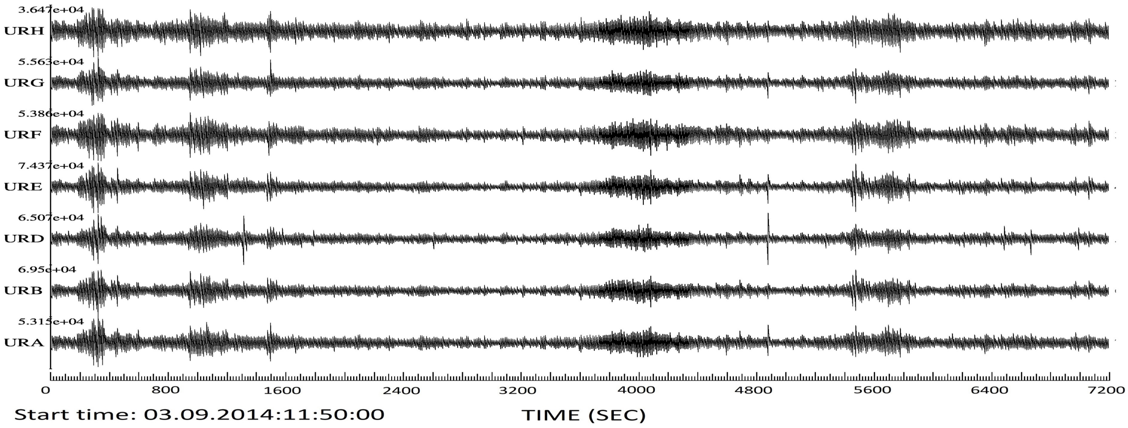

Fig. 5.2: Multichannel seismogram of 5L seismic array recorded on 3 September 2014 from 11:50:00 to 13:50:00.

value of power spectrum $\sim 1.3\,\mathrm{Hz}$.

Results of array data processing by SRP–PHAT using the settings described above are presented in Fig. 5.3. It is clearly seen that during 2 hours from 11:50:00 to 13:50:00 volcanic tremor laterally moved in an area of backazimuth from 120° to 140° and vertically with respect to slowness ranged from $0.44\,\mathrm{s\,km^{-1}}$ to $0.75\,\mathrm{s\,km^{-1}}$. According to *Eibl et al.* (2017), we got a perfect match for backazimuth estimates, but for slowness values they obtained estimates in shorter range – $[0.58; 0.75]$. Also, the authors presented an estimated dependency between slowness values and tremor source depth, so we can conclude that for found slownesses from $0.44\,\mathrm{s\,km^{-1}}$ to $0.75\,\mathrm{s\,km^{-1}}$ the tremor sources are distributed at depths from 0.4–0.5 to 2.3 km.

Detected 79 events for signals of which slowness values are in the range from 0.44 to 0.58 belong to volcanic tremor process, their backazimuth mostly in the same range from 120° to 140°, but they are more deep-focus and located at depths from approximately 1.8 km to 2.3 km. Moreover, these events are not the result of a false detection as shown in *f*–*k* maps of Fig. 5.4. The quality of the *f*–*k* maps indicates the presence of a coherent source signal.

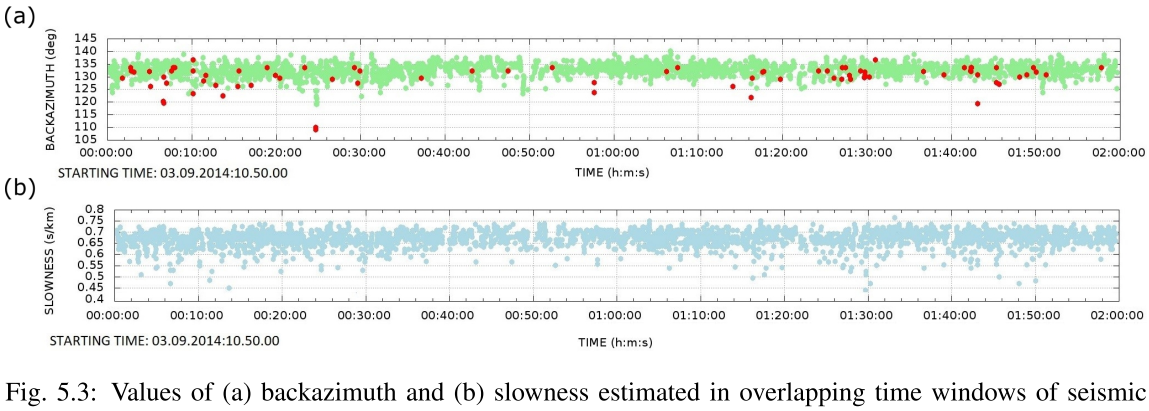

Fig. 5.3: Values of (a) backazimuth and (b) slowness estimated in overlapping time windows of seismic array data given in Fig. 5.2. Red and green points correspond to different slowness values in the ranges of $[0.44; 58)$ and $[0.58; 0.75]$ respectively.

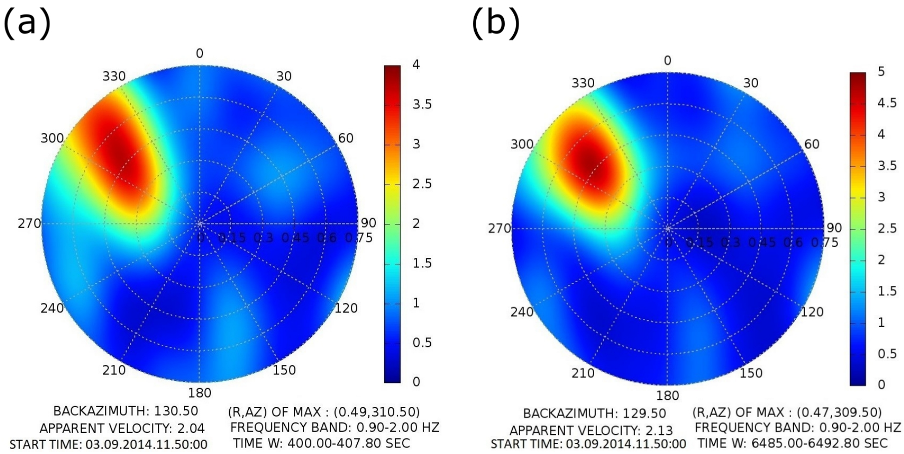

Fig. 5.4: Example of f–k maps calculated by SRP–PHAT of two detected events with wave slowness less than $0.58\,\mathrm{s\,km^{-1}}$.

6 *Microseismic source location with explosion focal mechanism*

This section is devoted to a simple numerical experiment with array data of perforation shots produced in a vertical oil well. All data and supplementary information necessary for array data processing was provided by the French corporation TOTAL E&P RECHERCHE DEVELOPMENT. We examined the application of the traditional semblance and SRP–PHAT methods for determining the lateral coordinates of a seismic source. Before, such experiments were performed only with synthetic (simulated) data, but here the idea is to confirm the results of surveys of past works, i.e., to approve advantage of the phase algorithm SRP–PHAT in accuracy estimation of microseismic source in completely real conditions.

Perforation shots are microseismic sources fired in a borehole before starting hydraulic fracturing. The focal mechanism is similar to explosion type – a uniform release of energy from a point source in all directions, so we should not worry about different polarities of P-waves caused by shear source radiation (*Staněk et al.*, 2015). The geometry of the 660 array sensors used for processing is given in Figure 6.1. The coordinates of the explosions in the borehole are known. There are ten explosions, distributed strictly vertically at depths from 2.642 km to 2.784 km. Since the coordinate origin was aligned with the wellhead location (Fig. 6.1), the horizontal coordinates of all explosions are $(0,0)$. For simplicity, only the horizontal coordinates were considered as unknown parameters, that is why we can calculate root square error (RSE) relatively to true position of source:

$$\mathrm{RSE}_k = \sqrt{(\theta_{1,k}-x_{0,k})^2+(\theta_{2,k}-y_{0,k})^2}\,, \quad k \in \overline{1,10}\,, \tag{6.1}$$

where $(\theta_{1,k},\theta_{2,k})$ is the estimate of the horizontal coordinates of the k^{th} perforation shot and $(x_{0,k},y_{0,k})$ its coordinates. According to a configuration of strictly vertical borehole and rectangular system in Fig. 6.1, $(x_{0,k},y_{0,k})=(0,0)$, $k\in\overline{1,10}$.

To calculate $\tau_k(\boldsymbol{\theta})$, $k=\overline{1,660}$, the horizontally homogeneous velocity model for P-waves was provided (Fig. 6.1b). A preliminary visual analysis of the multichannel seismo-

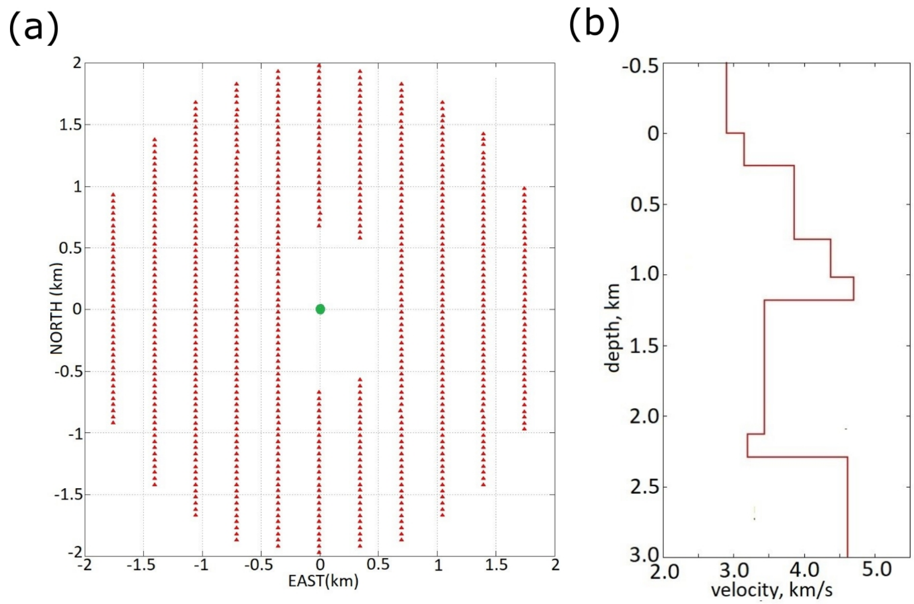

Fig. 6.1: (a) Layout of a total of 660 sensors of the array used for locations of the perforation shots. The green point denotes the borehole. (b) Local horizontally homogeneous velocity model for P-waves.

grams using bandpass 20 Hz to 50 Hz showed that the waveforms of the signal from perforations are completely or partially hidden under real noise. Thus, the need to use beamforming methods to locate the perforation shots is obvious. The interval of perforation shot signal, recorded by array sensors, is very short ~ 0.3 s to 0.4 s when taking into account the time delays of P-wave signals at array sensors and the local velocity model (Fig. 6.1b). The processing time window is set to 0.5 s. According to the formula (3.1), we are looking for maximum argument of objective function on the set $\Theta = [-0.3, 0.3] \times [-0.3, 0.3]$ with a grid step of 0.02 km.

Table 6.1: Estimation errors of perforation shots coordinates for SRP–PHAT and semblance methods.

Shot	Origin time	Depth (km)	SRP-PHAT RSE (km)	Semblance RSE (km)
P1	2012-04-13 05:57:30	2.784	0.044	0.35
P2	2012-04-17 17:41:47	2.756	0.028	0.02
P3	2012-04-18 19:40:08	2.736	0.028	0.24
P4	2012-04-23 18:29:19	2.693	0.020	0.02
P5	2012-04-23 18:29:49	2.692	0.040	0.02
P6	2012-04-23 18:30:19	2.691	0.028	0.02
P7	2012-04-23 18:30:49	2.690	0.020	0.02
P8	2012-04-25 13:54:24	2.669	0.020	0.02
P9	2012-04-25 13:56:24	2.660	0.028	0.02
P10	2012-04-25 14:07:24	2.642	0.028	0.02

Using multichannel records of seismic array determination of horizontal position by semblance and SRP–PHAT was applied to all 10 perforation shots. Results with error comparison are given in Table 6.1. In 8 out of 10 cases, both methods determined the

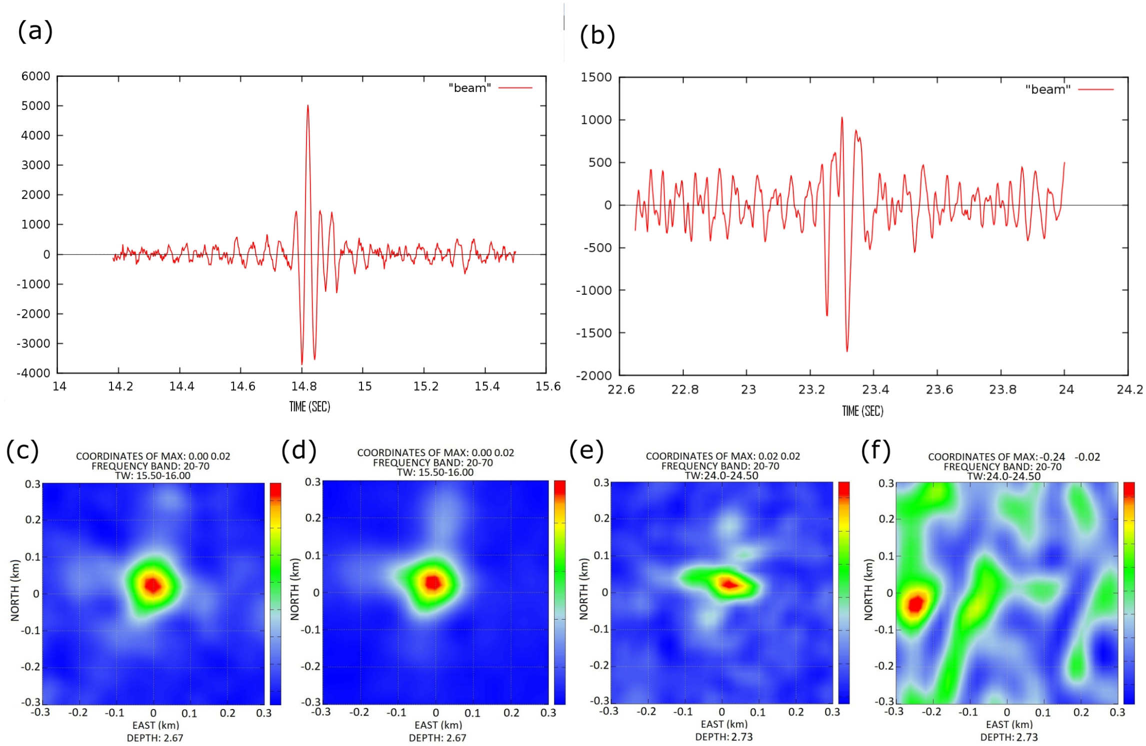

Fig. 6.2: Beams of perforation shots P-waves calculated by 660 multichannel array data: (a) Event P8; (b) Event P3; Location maps calculated by objective functions of different methods and for different events: c, e – SRP–PHAT, events P3 and P8 respectively; d, f – semblance, events P3 and P8 respectively.

source position accurately, but for events P1 and P3 (Table 6.1) the accuracy estimation of the semblance method dropped dramatically. To understand the reason for this, we built beams of P-waves for events P3 and P8 relative to the point $(0,0)$ – the true value of the source coordinates (Fig. 6.2). The beam represents the resulting signal from delay and sum of all 660 P-wave signals pre-filtered in the 20 Hz to 50 Hz frequency band. Beams can help to establish effectiveness of noise averaging by simple summation which is the basis of the semblance method. Location maps in Fig. 6.2 and as well as f–k maps are useful for analyses of method capability to accurately estimate source coordinates. The signal shape of beam for the P8 (Fig. 6.2a) event exactly repeats the so-called Ricker wavelet (*Ryan*, 1994), which is commonly used for synthetic seismogram calculation. Its excess over the noise level – tails of beam indicate a fairly high value of SNR, that is why there is no problem in accurately estimating the source coordinates by both semblance and SRP–PHAT methods (cf. Figs. 6.2c and 6.2d). Problems arise when the SNR of beam is rather poor, as can be seen for event P3 (Fig. 6.2b), where even the shape of perforation shot signal was distorted by seismic interferences. Even in this case, SRP–PHAT shows sufficiently high precision because of its robustness to noise characteristics (defined by $\dot{\mathbf{F}}_j$ in model (2.3)) in contrast to semblance, which clearly follows from the very poor quality of map Fig. 6.2f compared to Fig. 6.2e. Numerical indicators of the quality of maps are not given here, although the existence of such indicators and the possibility of calculation exist, as stated in the section on f–k analysis. The same situation of low SNR was obtained for P1 as can be seen from Table 6.1: the RSE value for semblance is equal to 0.35 km.

Finally, it should be noted that in practice of microseismic monitoring more often deals with seismic sources with complex focal mechanisms. It means that the stress field created by a source in the elastic earth's medium is described by the tensor of normal and tangential stresses. In this regard, the source exerts either compressive $(+)$ or tensile $(-)$ effects on the environment closest to it, and the polarities of the effects are generally different in different directions (at each fixed moment in time). Another feature of the problem under consideration is the uncertainty in the a priori knowledge of the radiation pattern of the microseismic source, which determines the amplitudes and polarities of signal oscillations recorded by seismic array sensors. Actually, there exists a solution described in *Staněk et al.* (2015), but they propose focal mechanism determination at first and then they suggest using semblance for source localization. This is a reasonable way, but still under the question of low SNR case. Hence, it would be better to adapt statistically based methods like SRP–PHAT to estimate source coordinates in case of complex mechanism. This is possible to do based on ideas of study *Kushnir et al.* (2014) and is the goal of the future research.

7 *Conclusions*

SRP–PHAT is a statistically robust estimator whose effectiveness has been demonstrated over many years in acoustics. In this paper, we consider this technique as a viable alternative to conventional seismic array data processing methods. The presented mathematical formulation justifies its applicability to f–k analysis and to the estimation of microseismic source coordinates using seismic array data.

Processing of seismic records from the ARCES array, including recordings of the explosion associated with the submarine accident on August 12, 2000, demonstrates the robustness of SRP–PHAT in estimating backazimuth and slowness compared to classical broadband f–k analysis. In particular, for the Sn phase, characterized by reduced spatial coherence, SRP–PHAT provides stable and physically consistent estimates, whereas CFK results show noticeable variability and ambiguity. Solving a similar problem for two hours of seismic records from the 5L array using overlapping time windows yields results consistent with *Eibl et al.* (2017), where deep volcanic tremor sources were identified with backazimuths ranging from 120° to 140°.

Numerical experiments with perforation shot data indicate improved performance of SRP–PHAT in estimating source coordinates compared to semblance. In several cases with low signal-to-noise ratio, conventional shift-and-sum procedures, which form the basis of semblance, do not provide sufficient noise suppression for accurate estimation.

Future work will focus on adapting the SRP–PHAT method for locating microseismic sources with complex focal mechanisms and on expanding its validation using additional low-magnitude seismic array datasets.

Acknowledgements

The author is supported by Contract DO-321/30.11.2023 *NGIC – National Geoinformation Center for monitoring, assessment and prediction of natural and anthropogenic risks and disasters*, funded by the Ministry of Education and Science of Bulgaria. The author is grateful to the TOTAL E&P RECHERCHE DEVELOPMENT corp. (France) for providing seismic array records of perforation shots processes, also author expresses gratitude for assistance and support with this data to members of ISTI inc. (USA) Mikhail Rozhkov and Ilya Dricker.

References

Aki, K. and P. G. Richards, 2009. *Quantitative seismology*. 2. edition, corrected printing. Mill Valley, California New York: University Science Books. 700 pp. ISBN: 978-1-891389-63-4.

Azzola, J. and E. Gaucher, 2024. Seismic Monitoring of a Deep Geothermal Field in Munich (Germany) Using Borehole Distributed Acoustic Sensing. *Sensors*, **24** (10), 3061. ISSN: 1424-8220. DOI: 10.3390/s24103061.

Brandstein, M. and D. Ward, eds., 2001. *Microphone arrays: signal processing, techniques and applications*. Digital signal processing. Berlin Heidelberg: Springer. 398 pp. ISBN: 978-3-540-41953-2.

Brokešová, J. and J. Málek, 2018. Small-aperture seismic array data processing using a representation of seismograms at zero-crossing points. *Physics of the Earth and Planetary Interiors*, **280**, 53–68. ISSN: 00319201. DOI: 10.1016/j.pepi.2018.04.010.

Dai, Y. and C. Sun, 2023. Adaptive Beamforming with Hydrophone Arrays Based on Oblique Projection in the Presence of the Steering Vector Mismatch. *Journal of Marine Science and Engineering*, **11** (4), 876. ISSN: 2077-1312. DOI: 10.3390/jmse11040876.

Duncan, P. M. and L. Eisner, 2010. Reservoir characterization using surface microseismic monitoring. *Geophysics*, **75** (5), 139–146. DOI: 10.1190/1.3467760.

Duncan, P. M., J. Lakings and R. Flores, 2010. “Method for passive seismic emission tomography”. Pat. #7,663,970.

Eibl, E. P. S., C. J. Bean, K. S. Vogfjörd, Y. Ying, I. Lokmer, M. Möllhoff, G. S. O’Brien and F. Pálsson, 2017. Tremor-rich shallow dyke formation followed by silent magma flow at Bárðarbunga in Iceland. *Nature Geoscience*, **10** (4), 299–304. ISSN: 1752-0894, 1752-0908. DOI: 10.1038/ngeo2906.

Eisermann, A. S., A. Ziv and H. G. Wust-Bloch, 2018. Array-Based Earthquake Location for Regional Earthquake Early Warning: Case Studies from the Dead Sea Transform. *Bulletin of the Seismological Society of America*, **108** (4), 2046–2053. ISSN: 0037-1106, 1943-3573. DOI: 10.1785/0120170315.

Gibbons, S. J. and F. Ringdal, 2006. The detection of low magnitude seismic events using array-based waveform correlation. *Geophysical Journal International*, **165** (1), 149–166. ISSN: 0956540X, 1365246X. DOI: 10.1111/j.1365-246X.2006.02865.x.

Grinstein, E., E. Tengan, B. Çakmak, T. Dietzen, L. Nunes, T. Van Waterschoot, M. Brookes and P. A. Naylor, 2024. Steered Response Power for Sound Source Localization: a tutorial review. *EURASIP Journal on Audio, Speech, and Music Processing*, **2024** (1), 59. ISSN: 1687-4722. DOI: 10.1186/s13636-024-00377-z.

Husebye, E. S. and A. M. Dainty, 1995. *Monitoring a Comprehensive Test Ban Treaty*. NATO ASI Series, Series E: Applied Sciences 303. Dordrecht: Springer. 864 pp. ISBN: 978-94-011-0419-7. DOI: 10.1007/978-94-011-0419-7.

Kennett, B. L. N., 2002. *The Seismic Wavefield: Volume II: Interpretation of seismograms on regional and global scales*. Cambridge: Cambridge University Press. 548 pp. ISBN: 978-0-521-00665-1. DOI: 10.1017/9781108780155.

Kushnir, A. F., A. V. Varypaev, M. V. Rozhkov, A. G. Epiphansky and I. Dricker, 2014. Determining the microseismic event source parameters from the surface seismic array data with strong correlated noise and complex focal mechanisms of the source. *Izvestiya, Physics of the Solid Earth*, **50** (3), 334–354. ISSN: 1069-3513, 1555-6506. DOI: 10.1134/S1069351314030033.

Kværna, T. and F. Ringdal, 1986. Stability of various f-k estimation techniques. 1-1986/1987. Kjeller, Norway: NORSAR, 29–40.

Legaz, A., A. Revil, P. Roux, J. Vandemeulebrouck, P. Gouédard, T. Hurst and A. Bolève, 2009. Self-potential and passive seismic monitoring of hydrothermal activity: A case study at Iodine Pool, Waimangu geothermal valley, New Zealand. *Journal of Volcanology and Geothermal Research*, **179** (1), 11–18. ISSN: 03770273. DOI: 10.1016/j.jvolgeores.2008.09.015.

Liu, F., Y. Wang, M. Kou and C. Liang, 2024. Applications of Microseismic Monitoring Technique in Coal Mines: A State-of-the-Art Review. *Applied Sciences*, **14** (4), 1509. ISSN: 2076-3417. DOI: 10.3390/app14041509.

Monzingo, R. A., T. W. Miller and R. L. Haupt, 2011. *Introduction to Adaptive Arrays*. 2nd ed. Electromagnetics and Radar Ser v.02. Raleigh: Institution of Engineering & Technology. 559 pp. ISBN: 978-1-891121-57-9.

Ryan, H., 1994. Ricker, Ormsby, Klauder, Butterworth – A Choice of Wavelets. *CSEG Recorder*, **19** (7), 8–9.

Schweitzer, J., J. Fyen, S. Mykkeltveit, S. J. Gibbons, M. Pirli, D. Kühn and T. Kværna, 2012. Seismic Arrays. *New Manual of Seismological Observatory Practice 2 (NMSOP2)*. Ed. by P. Bormann, 1–80. DOI: 10.2312/GFZ.NMSOP-2_CH9.

Silverman, H., Ying Yu, J. Sachar and W. Patterson, 2005. Performance of real-time source-location estimators for a large-aperture microphone array. *IEEE Transactions on Speech and Audio Processing*, **13** (4), 593–606. ISSN: 1063-6676. DOI: 10.1109/TSA.2005.848875.

Staněk, F., D. Anikiev, J. Valenta and L. Eisner, 2015. Semblance for microseismic event detection. *Geophysical Journal International*, **201** (3), 1362–1369. ISSN: 1365-246X, 0956-540X. DOI: 10.1093/gji/ggv070.

Varypaev, A., 2024. Asymptotic Form of the Covariance Matrix of Likelihood-Based Estimator in Multidimensional Linear System Model for the Case of Infinity Number of Nuisance Parameters. *Mathematics*, **12** (3), 473. ISSN: 2227-7390. DOI: 10.3390/math12030473.

Varypaev, A. and A. F. Kushnir, 2020. Statistical synthesis of phase alignment algorithms for localization of wave field sources. *Multidimensional Systems and Signal Processing*, **31** (4), 1553–1578. ISSN: 0923-6082, 1573-0824. DOI: 10.1007/s11045-020-00722-3.

Zhang, C., D. Florencio, D. Ba and Zhengyou Zhang, 2008. Maximum Likelihood Sound Source Localization and Beamforming for Directional Microphone Arrays in Distributed Meetings. *IEEE Transactions on Multimedia*, **10** (3), 538–548. ISSN: 1520-9210, 1941-0077. DOI: 10.1109/TMM.2008.917406.